Study of the hydrogen uptake in deformed steel using the microcapillary cell technique

Ozdirik, Berk; Suter, Thomas; Hans, Ulrik; Depover, Tom; Verbeken, Kim; Schmutz, Patrik; Jeurgens, Lars P.H.; Terryn, Herman; De Graeve, Iris

Published in:
Corrosion Science

DOI:
10.1016/j.corsci.2019.04.029

Publication date:
2019

Document Version:
Accepted author manuscript

Study of the hydrogen uptake in deformed steel using the microcapillary cell technique

Berk Ozdirik [a,b,c], Thomas Suter [c], Ulrik Hans [c], Tom Depover [b], Kim Verbeken [b], Patrik Schmutz [c],

Lars Jeurgens [c], Herman Terryn [a], Iris De Graeve [a,b]

[a] *Research Group Electrochemical and Surface Engineering (SURF), Department of Materials and Chemistry, Vrije Universiteit Brussel, Pleinlaan 2, B-1050 Brussel, Belgium*

[b] *Department of Materials, Textiles and Chemical Engineering, Ghent University (UGent), Technologiepark 903, B-9052 Ghent, Belgium*

[c] *Laboratory for Joining Technologies and Corrosion, Empa, Swiss Federal Laboratories for Materials Science and Technology, Überlandstrasse 129, CH-8600 Dübendorf, Switzerland*

Abstract

Steel manufacturing processes can induce high deformation (strain) in the microstructure of high strength steels, making them more susceptible to hydrogen embrittlement. It is crucial to investigate the impact of the manufacturing process on the local hydrogen uptake in steel. The microcapillary cell electrochemical method is capable of evaluating the hydrogen uptake in steel as a function of the deformation which is induced by various mechanical methods, i.e cold rolling, bending and punching. A clear relation between the deformation degree and the local hydrogen content is established for a dual phase (DP600) steel. Going towards microscale investigations of punched samples, the analysis of the deformed zones nearby the punched edge by a combination of optical microscopy, scanning electron microscopy and micro hardness measurement provide additional information on the microstructural characteristics of these highly deformed zones. Furthermore, the magnitude of the deformation nearby the punched edge is quantitatively determined by means of electron backscatter diffraction technique. A shear affected zone is identified at the edge of the punched hole, where excessive deformation and a higher dislocation density are present. The dedicated local electrochemical measurements confirm the presence of a high amount of local hydrogen in this shear affected zone, which is likely detrimental for hydrogen embrittlement.

1. Introduction

In the last two decades, the increasing demand of the automotive industry to lower the car weight together with an increase in strength and stiffness of the steel used in the car body has been fulfilled by the development of advanced high strength steels. However, these high strength steels are reported to be susceptible to hydrogen embrittlement. **[1-4]** The possibility for steels to come into contact with hydrogen containing environments during manufacturing or in use, opens the path for hydrogen to enter the steel microstructure. After hydrogen entry into the steel microstructure, it is distributed between interstitial sites in the lattice (lattice mobile hydrogen) or trapped near microstructural inhomogeneities such as dislocations, grain boundaries, interfaces, vacancies, etc.. **[5]** Depending on the activation energy (E) of the trapping sites, traps can be classified as reversible (E<60 kJ/mol) or irreversible (E>60 kJ/mol) hydrogen traps. **[6]** In the literature, there is an additional term, “diffusible hydrogen” defined by *Akiyama* as the one

which can be determined by heating the sample up 300^0C **[7-8]**, which includes lattice mobile hydrogen and reversibly trapped hydrogen.

Hydrogen trapping at microstructural features has an effect on the diffusion process. During hydrogen diffusion, hydrogen is distributed between lattice and trap sites; as such an equilibrium is attained between interstitial hydrogen and trapped hydrogen. **[9]** To describe the transport of hydrogen influenced by the traps, an apparent hydrogen diffusion term is commonly used in the literature. **[10]** For instance, *Zakroczmski et al.* **[11]** studied pure iron subjected to simultaneous hydrogen charging and straining. He reported that dislocations act as traps for hydrogen, and thus decrease the apparent hydrogen diffusivity. Dislocations are considered to be reversible traps with an intermediate binding energy of 20.2 kJ/mol. **[12]** The dislocation trap density in the steel microstructure increases with plastic straining. However, it should be pointed out that dislocation trap densities show variation within the microstructure, depending on the degree of local plastic strain. **[9]** Thus, hydrogen accumulates at dislocations where local plastic deformation occurs. **[13]** Moreover, *Kumnick et al.* indicated that increasing the degree of cold-work on iron can result in an increase of the binding energy of hydrogen to dislocations to hydrogen as well as the intensity of the dislocation density. **[14]**

Plastic deformation is reported to induce additional potential reversible traps for hydrogen in the steel microstructure. **[15-16]** Therefore, applied strain is considered important in terms of hydrogen embrittlement. In the mass production of automotive parts and components, sheet metal forming processes (such as bending, punching etc.) are commonly used. **[17]** Cold forming techniques can induce high magnitude of local deformation regions, where hydrogen can be possibly trapped during in-service condition as a result of the hydrogenation reaction. Once the hydrogen concentration reaches a critical value inside the steel, it can lead to a strong reduction of its mechanical properties, i.e. a hydrogen induced ductility loss. **[18]** In other words, interstitial mobile and reversibly trapped hydrogen are considered to be detrimental hydrogen sources for hydrogen induced cracking. **[19-24]**

To have a better understanding of hydrogen induced cracking phenomena in steel with respect to hydrogen concentration, various hydrogen measurement methods have been developed. Hydrogen/trap interactions can be identified by thermal desorption spectroscopy (TDS). This technique determines the hydrogen desorption flux upon heating a sample and aims at discriminating between various possible hydrogen traps releasing the hydrogen at different temperatures corresponding to different trap binding energies.**[19-25]** In addition, the diffusible hydrogen content in steel can be determined by hot extraction, **[26]**, while the total hydrogen content can be measured by melt extraction. **[26-28]** Apart from these thermal methods, the electrochemical approaches have recently gained importance to investigate lattice dissolution and microstructural trapping of hydrogen in iron and its alloys. Electrochemical permeation

methods can provide reliable information on diffusivity and solubility of hydrogen in steel, as first elaborated by *Devanathan*,**[29]** and further explored in various studies.**[30-33]** Additionally, the electrochemical potentiostatic oxidation technique has been used in some studies **[34-36]** to measure the hydrogen uptake in steel, and also a cyclic voltammetry method was recently elaborated **[37]**. It can be summarized that thermal hydrogen measurements as well as the electrochemical methods are capable of observing and quantifying the hydrogen content within the sample volume. However, generally speaking, hydrogen is not homogeneously distributed within a steel microstructure since its local distribution is very much related to local microstructural features (i.e. strain distribution, phases, etc..).

Local hydrogen concentration measurements in a steel microstructure play a crucial role in understanding hydrogen embrittlement.**[38-39]** It is essential to reveal quantitative relationships between local strain and the corresponding local hydrogen content. With the microcapillary cell technique **[40-43],** reliable information concerning the local hydrogen content can be obtained with high spatial resolution. The microcapillary cell allows electrochemical measurements on sample surface regions of interest, where specific microstructural features are present, with dimensions in the micro- or sub micrometer range. **[44]** This local electrochemical hydrogen measurement method are claimed to be capable of measuring the trapped hydrogen in steels, which could be detected quite accurate after days, weeks or even years after hydrogen uptake. **[45-46]** *Shinozaki et al.* **[47]** used this method to investigate the microstructural distribution of hydrogen uptake in steel and saw that MnS inclusions can trap hydrogen, causing hydrogen embrittlement. Further, *Fushimi et al.* **[48]** incorporated a microcapillary cell technique into a Devanathan-Stachurski electrochemical cell for local measurement of hydrogen permeation of a steel sheet. *Kühn et al.* **[45]** used the microcapillary cell technique with the aim of quantifying the local hydrogen level in a notched tensile steel sample. In this study, the local hydrogen level was found to be higher in the regions exposed to high stresses compared to the regions with low/no stress. Similarly, *Manke et al.* **[46]** used the technique to quantify hydrogen uptake and found a good correlation with the results obtained by conventional hydrogen analysis methods. However, in this study, no direct link between local strain level and local hydrogen content was established.

Local strain enhancements in steel need to be examined since hydrogen embrittlement is believed to occur preferably in strain-localized regions in the steel. **[49-50]** To do so, an experimental method to measure and map the localized strain distribution is desired. EBSD can provide a means of determining local strains in combination with having high spatial resolution and good strain sensitivity. **[51-52]** By means of this technique, misorientations in polycrystals can be mapped using several different kinds of metrics to visualize plastic deformation around cracks, inside deformed grains etc. **[53]** In this regard, *Nakada et al.* **[54]** used this technique to map the deformation locally distributed in dual phase steel after deformation processes, i.e. cold-rolling and punching. In this study, the quantification of the local deformation within the punched

zone is also performed based on the change in crystal rotation angle as a result of the applied deformation.

It is known that dual phase (DP) steels are subjected to heat treatments during their production process and such treated steel microstructures can have many potential trap sites for hydrogen. For instance, DP600 steel alloys consist of ferrite and martensite phases, where hydrogen can be potentially trapped at phase boundaries, in addition to grain boundaries, dislocations, and lattice vacancies. **[55-56]** *Kozekwa et al.* **[57]** stated that as-received dual phase steel contains low average dislocation density. It was further reported that with increasing plastic deformation, the crystal rotation angle, namely the misorientation between the grains, is changed; as such the average dislocation density in the microstructure increases. Similarly, *Ruiz-Andres* **[58]** demonstrated that the microstructure of as-received DP steel has weak misorientation within the ferrite grains, implying low dislocation density. More importantly, it was revealed that the microstructure of the bent specimen exhibit a severe plastic deformation mainly localized within the ferritic matrix and in the vicinity of the ferrite/martensite grain boundaries. In the study of *Kapp*, **[59]** it was demonstrated that when the magnitude of the applied global deformation increases, the network-like structure of local strain band appears in the steel microstructure.

In the study of *Takagi et al.* **[18]**, it was proven that the application of a bending process induces a high amount of strain in the steel, which increases the trapped hydrogen content. In the study of *Yoshino et al.* **[60]**, in-depth microstructural characterization of bended steel is performed in addition to hydrogen measurement by thermal desorption analysis, proving that the bending process creates shear affected zones in the steel microstructure, where high amounts of hydrogen can locally accumulate. In the study of *Wu et al.* **[61],** the microstructural characterization of punched dual phase steel was performed and a shear affected zone in its microstructure was clearly identified. Additionally, strain distribution measurements confirmed that the magnitude of shear strain was very high at the edge of the punched hole and that it decreased rapidly away from the edge. Similarly*, Yokoi et al* **[62]** measured very high strain values near the punched hole edge, where a very fine grain microstructure is observed compared to the average grain size in the bulk. In the study of *Nakada et al.*, **[54]** it was also proven that the region with large strain is localized in the vicinity of the punched edge. Further, *Scharf et al.*, **[63]** indicated that the punching process can create shear affected zones around the punched edge, where grain deformation and a higher dislocation density arise. It was also demonstrated by means of a constant load test that this zone is highly susceptible to hydrogen embrittlement. In the further study *of Scharf et al.*, **[64]** trapped hydrogen concentration of the punched steel bulk was determined by thermal desorption analysis after being exposed to a corrosive hydrogen charging environment. However, in this study, the difference between hydrogen uptake capacity of deformed and non-deformed microstructures was not addressed.

To summarize, various electrochemical and thermal hydrogen measurements are possible to evaluate the risk of hydrogen embrittlement where the metal is locally deformed to a high extent in high strength steels after manufacturing processes. Obtaining information concerning local distribution of trapped hydrogen is of great importance. The microcell technique allows for performing electrochemical measurements on areas with dimensions in the micrometer range. Since it is being used in direct combination with optical microscopy of the area to be electrochemically characterized, it enables to precisely position the microcell on the region of interest. Moreover, the complementary use of scanning electron microscopy (SEM), provides additional information regarding the microstructural features, and as such a direct relation can be established between local strain and the local hydrogen content. Moreover, this method is non-destructive and does not modify the steel microstructure.

The objective of the present study is to demonstrate the method sensitivity (lateral, hydrogen concentration) by determining the local hydrogen concentration in deformed steel. The impact of plastic deformation (cold rolling, bending and punching) on the hydrogen uptake capacity is evaluated by the micro-cell electrochemical method using conventional capillaries (*inner diameter of 160 µm*). To obtain specific information regarding the local hydrogen concentration within a highly deformed region, more local microcell measurements are carried out using smaller capillaries (*inner diameter of 10 µm*). The procedure involves first electrochemical charging of hydrogen in the steel samples, followed by local microcell discharging experiments. From the discharging curves obtained, the amount of charge released is calculated based on Faraday's law. This allows determining the amount of trapped hydrogen being oxidized during discharging. Three types of deformation are introduced: i) macroscopic deformation through cold rolling where the whole sample experiences deformation; ii) local bending effect; and iii) local punching effect introducing very high local strain levels around the punch hole. To quantitatively evaluate the magnitude of strain around the punched hole, electron backscatter diffraction (EBSD) analysis is carried out. Lastly, to establish a link between the mechanical properties and microstructural features, micro hardness measurements are conducted nearby the punched hole.

2. Material Characterization

Dual Phase steel (DP600) is used for this study, for which the chemical composition is listed in Table 1. The steel microstructure comprises approximately 23% of martensite and 77% of ferrite, with a grain size of about *7 µm* for the ferritic phase and about *2 µm* for the martensitic phase. **[65-66]**

Table 1. Chemical composition of the material of interest

Materials	**Composition (wt %, Fe balance)**

DP600	0.07 C, 1.5 Mn, 0.25 Si, 0.4-0.8 Cr+Mo

The thickness of the DP steel sheet was 1.1 mm. This thickness was reached after hot and cold rolling, followed by subsequent annealing using industrial annealing parameters necessary to obtain the desired dual phase microstructure. The steel is delivered as a sheet and cut into square samples of 2 cm x 2 cm. The samples are mechanically ground with SiC paper up to 1000 grit paper. The final thickness of the samples after grinding is 0.9 mm. To remove surface contamination prior to the electrochemical experiments, the samples are placed in an ultrasonic bath, cleaned with ethanol for 3 minutes and subsequently dried by gently wiping with a clean tissue. It has to be further mentioned that after the punching process, the steel sample is additionally ground with 1000 grit paper to eliminate the burr and the micro cracks on the surface, which are formed around the punched hole.

The microstructures of the non-deformed as well as punched steel samples are observed by means of optical microscopy, which is attached to the micro-capillary cell, and by scanning electron microcopy (SEM). Prior to microstructural characterization, the steel samples are etched with 2% Nital solution in order to identify the phases present. SEM investigations are performed with a JEOL JSM-IT300 system; images are collected in secondary electron mode, with an acceleration voltage of 5 kV.

To determine the magnitude of deformation near the punched edge, EBSD analysis is performed using a field emission scanning electron microscope. The captured EBSD patterns are analyzed by the OIM software. EBSD-KAM (kernel average misorientation) was determined by first nearest-neighbor points under a condition that a misorientation angle larger than 5° is not taken into account. The change in the KAM values due to the punching process is considered as an indicative measure for the deformation. To quantify the magnitude of the equivalent strain (deformation) induced by the punching nearby the punched edge, the following power law determined on a similar dual phase steel, reported by *Nakada. et al.*, **[54]** is used:

$$\theta_{KAM} = \frac{\pi}{180}\, 1.68\, \varepsilon^{0.44} \text{ (rad)} \tag{1}$$

Using this formula, the calculated KAM values θ_{KAM} can be translated into the equivalent strain ε.

3. Experimental Procedure

3.1 Micro-electrochemical Procedure

The experimental procedure is comprised of three main sections: mechanical deformation, hydrogen charging and hydrogen discharging. The procedure starts by inducing a certain

mechanical deformation by means of rolling, bending or punching, and is subsequently followed by an hydrogen charging step. It is important to indicate that the hydrogen charging step is performed on a macroscopic scale, while hydrogen discharging is characterized on microscopic scale in relation to different specific microstructures.

3.1.1 Mechanical Deformation

To introduce plastic deformation in the steel samples, three different mechanical deformation methods are used: rolling, bending and punching.

- ***Cold-Rolling***

Cold deformation of 4 and 11% was applied on the as-received steel to induce macroscopic averaged scale deformation in the material.

- ***3 Point Bending Test***

A three point bending cell configuration, consisting of a standardized procedure adopted from the study of *Breimesser et al.*, **[67]** is used to plastically deform steel by applying constant stress (up to 160% of the tensile strength of steel) by means of a screw, as schematically illustrated in figure 1. On top of the bended steel sheet, an electrochemical cell is placed to carry out hydrogen charging. The corresponding procedure is explained in the next section.

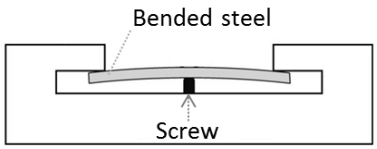

Figure 1- Schematic representation of bending test

- ***Punching Test***

A steel sample is punched by means of a punching machine, shown in figure 2.a, and a round-shaped hole (diameter of 3 mm) is created in the sample at the end of this process, as depicted in figure 2.b.

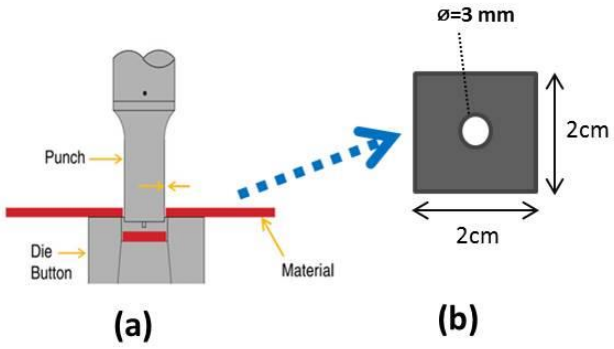

Figure 2- Schematic presentation of a) the punching test and b) the punched steel sample

3.1.2 Hydrogen Charging

The steel specimens are charged with hydrogen in an electrochemical cell filled with 0.2 M NaOH solution containing 1 g/l thiourea (hydrogen recombination poison) by applying a galvanostatic cathodic polarization at a current density of $10\ mA/cm^2$ for 2 hours.

Depending on the type of sample investigated, hydrogen charging is performed in three different electrochemical setups. Non-deformed and cold-rolled steel samples are hydrogen charged in a macroscopic electrochemical cell, as shown in figure 3.a, using a three electrode configuration: the steel sample as working electrode (W.E.), saturated calomel electrode within luggin capillary as reference electrode (R.E) and a platinum grid as counter electrode (C.E). For bended steel samples, as shown in figure 3.b, a polymer based sealing ring is placed on the deformed area and charging is carried out in an electrolyte using the three electrode configuration with the steel sample as W.E, a stainless steel wire as R.E. and a stainless steel wire as C.E. In the last electrochemical setup, as shown in figure 3.c, the punched steel sample is fully immersed in the electrolyte so that hydrogen charging is performed using again the steel sample as W.E, a saturated calomel electrode within luggin capillary as R.E and a stainless steel wire as C.E.

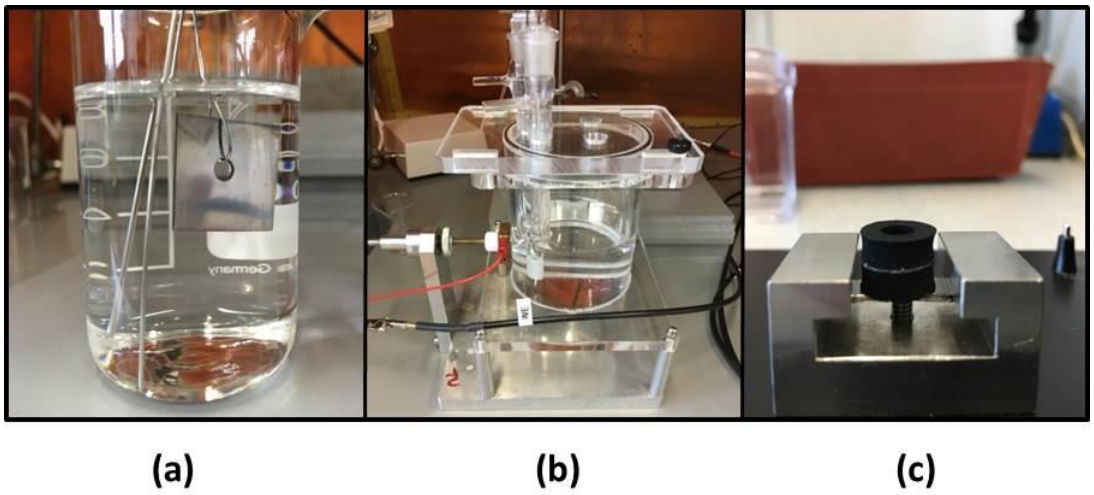

Figure 3- Pictures of the hydrogen charging setups a) macro-cell for non-deformed and 4, 11% cold-rolled steel samples, b) for bended samples, c) punched samples

After H-charging, the charged specimens are immediately taken out of the cell, flushed with double distilled water and ethanol and then dried by means of wiping with a clean tissue. Afterwards, the vicinity of the exposed area to H-charging in the specimen is marked with a blade so that the exposed area can be recognized during H-discharging measurement. The sample is stored in a desiccator for 2 hours before the discharging procedure to determine the trapped hydrogen content.

3.1.3 Hydrogen Discharging and Concentration Quantification

Hydrogen discharging is performed by the micro-cell technique. The micro-cell equipment consists of a glass tube with a tip sealed by a layer of silicon rubber, a counter electrode with a 0.5 mm thick platinum wire and a saturated calomel electrode as a reference electrode. The micro-capillary glass is connected to a reference electrode by an electrolyte bridge filled with 0.2 M concentration of NaOH solution.

Prior to H-discharging, the steel specimen is freshly ground with 1000 grit paper for 5 seconds to minimize oxide layer formation as a result of sample disassembly after hydrogen charging. This is followed by rinsing with ethanol and subsequent drying with a clean tissue.

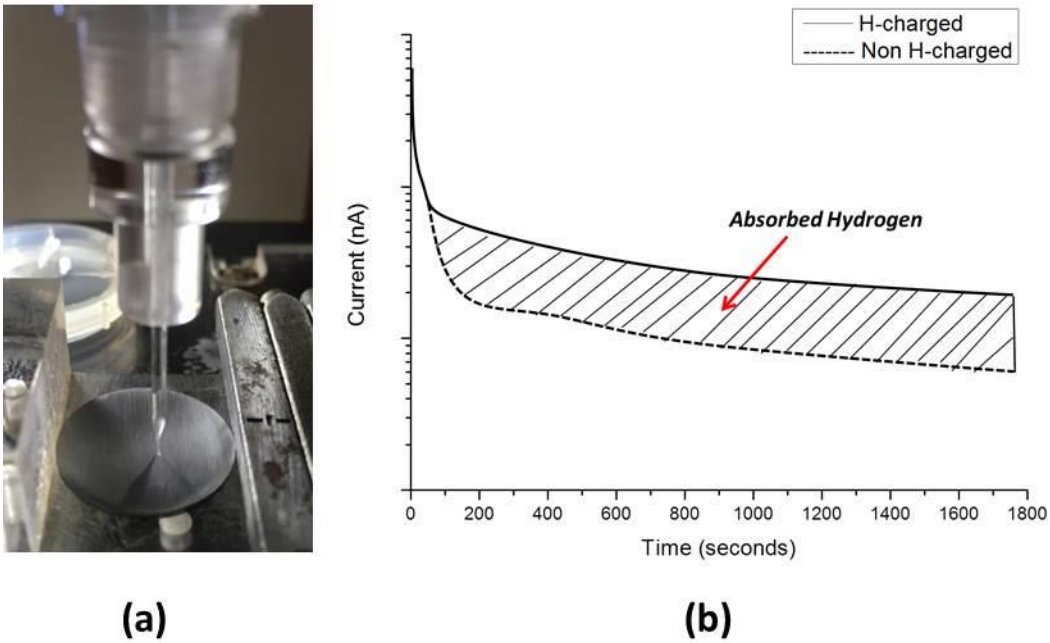

Figure 4- a) Illustration of micro-cell setup for discharging measurements and b) schematic representation of current-time transient recorded during hydrogen discharging

The capillary cell is mounted on the revolving nosepiece of an optical microscope. This setup enables the microscope to be used to locate the region of interest in the sample' microstructure and also a precise positioning of the micro-cell on that position of interest.

To perform H-discharging measurements, as shown in figure 4.a, the micro-capillary is gently placed onto the surface of the specimen (working electrode) in such a way that only the inner area of the capillary opening is exposed to the electrolyte. The sample is then potentiostatically polarized by applying an anodic potential of +0.3 V vs. saturated calomel electrode (SCE) for 30 minutes. Note that, in this study, two different pulled micro capillary sizes having inner diameters of *10 µm* and *160 µm* are used.

For the H-discharging measurements, a high resolution potentiostat with a current detection limit of 1 fA is used. To shield the electrochemical setup from electromagnetic and acoustic interference, the measurements are performed in a Faraday cage. During the measurement, the change in anodic current with time is recorded, as shown in figure 4.b, so that the integration of this resulting curve can provide the amount of charge released after H-charging ($Q_{H-charg}$) and without H-charging (Q_{Non-H}), respectively. One should note that this applied H-discharging method forces the hydrogen level to be on the zero on the measured spot, so the equilibrium is reset between the reversibly trapped and lattice hydrogen. Thus, during H-discharging procedure, the trapped hydrogen is liberated from its trapping site and becomes mobile hydrogen. **[45-46]**

According to the Faraday formula (2), the concentration of trapped hydrogen being oxidized during H-discharging can be calculated, as indicated below:

$$C_H = \frac{Q_{H-charg} - Q_{Non-H}}{n\,F\,V} \quad (2)$$

In formula (2), C_H is the trapped hydrogen concentration in steel, *n* is the number of electrons participating in the oxidation reaction of trapped hydrogen; *F* is the Faraday constant (96485 C/mol), and *V* is the effective diffusion volume. According to formula (2), the number of electrons corresponding to the hydrogen discharging reaction ($H \rightarrow H^+ + e^-$) is considered to be 1. Moreover, the effective diffusion volume is considered to have a half-ellipsoidal shape, which depends on the radius of the microcapillary used for the measurement and the diffusion distance of hydrogen, as such it can be calculated according to the formula below:

$$\frac{V}{2} = \frac{4}{6}\,(a + L_D)^2\,L_D \quad (3)$$

In formula (3), L_D is the diffusion distance of hydrogen, *a* is the radius of the microcapillary. Further, the diffusion distance of hydrogen is calculated according to the Fick's Law formula below:

$$L_D = \sqrt{D_H\,t} \quad (4)$$

In formula (4), t is the time for hydrogen discharging (1800 seconds), while D_H stands for the effective diffusion coefficient of hydrogen in steel. Diffusion coefficient of hydrogen for non-deformed dual phase (DP600) steel is 7.65×10^{-7} cm^2/s. **[65]**, **[68]** The diffusion coefficient of hydrogen in steel is assumed to decrease with increasing amount of plastic deformation, as widely accepted in the literature. **[69-73]** Considering the relation of the H-diffusion coefficient to the degree of cold-rolling reported by *Huang* et al, **[73]** the H-diffusion coefficient for 4% and 11% cold-rolled steels is calculated to be 6.37×10^{-7} cm^2/s and 5.10×10^{-7} cm^2/s, respectively. Therefore, using formula (4), for the micro (d_{inner}=160 µm) measurements, the effective diffusion distance of hydrogen for non-deformed, 4% cold-rolled and 11% cold-rolled is calculated to be 370 µm, 330 µm and 302 µm, respectively. Moreover, for the local (d_{inner}=10 µm) and micro (d_{inner}=160 µm) measurement of the region nearby the punched hole, the corresponding hydrogen diffusion coefficients with respect to the magnitude of deformation are considered to be 10^{-8} cm^2/s and 1.4×10^{-7} cm^2/s; as such, the diffusion distances of hydrogen are calculated to be 42 µm and 158 µm, respectively.

3.2 Micro-hardness measurement procedure

The micro-hardness measurements were performed on a cross-section of a punched steel with a load of 30 grams for 20 seconds using a Fischerscope® HM2000 micro hardness tester. The measurement is initiated from the vicinity of the punched edge towards the interior of the steel with a distance of *56 µm* between each measurement point.

4. Results and Discussion

4.1 Influence of various mechanical deformation processes on the H-uptake in steel

To test the influence of mechanical deformation on H-uptake, steel samples are subjected to different metal forming processes (rolling, bending and punching) before cathodic hydrogen charging. Considering the deformation characteristics of each process, the influence of mechanical deformation on the hydrogen trapping/release is evaluated in two sub-sections:

4.1.1Influence of the degree of cold rolling on the trapped hydrogen content

To establish a relation for the effect of cold-rolling on the concentration of trapped hydrogen in steel, cold-rolled (4 and 11%) steel sheets have been analyzed by micro-cell (d_{inner}=*160 µm*) after having been hydrogen charged for 2 hours in 0.2 M NaOH solution containing 1 g/l thiourea .

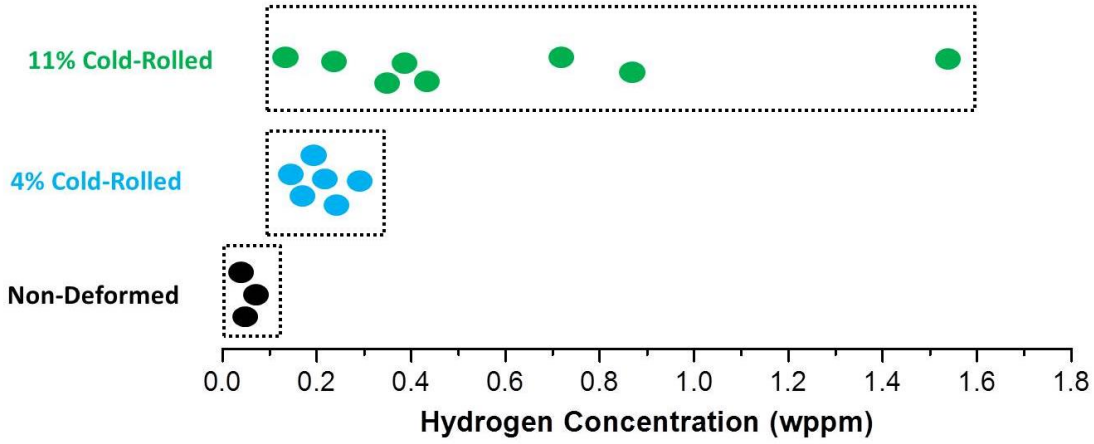

Figure 5- Calculated hydrogen concentrations obtained from the current transient integration in non-deformed and cold-rolled samples (4%, 11%) as determined from micro-cell analyses (d_{inner}=*160 µm*) after H-charging for 2 hours in 0.2 M NaOH solution containing 1 g/l thiourea

In figure 5, the calculated hydrogen concentration obtained from the integration of the discharging current transients and corrected according to the formula 2 are compared for the non-deformed and cold-rolled samples. The trapped hydrogen concentration clearly increases (on

average) with increasing degree of cold rolling, as well as the hydrogen concentration range of the measured data points. For 11% cold-rolled steel, estimated hydrogen concentration values are distributed over a larger range [0.1-1.6 wppm] compared to the 4% cold-rolled steel [0.1-0.3 wppm]. This larger variation in hydrogen content can indicate that the strain induced by cold work is distributed heterogeneously over the steel microstructure, a relation which will be further addressed in the discussion section.

4.1.2Influence of local metal deformation processes (Bending, Punching) on the trapped hydrogen content

In table 2, the calculated hydrogen concentration ranges based on the current transients for non-deformed, bended and punched samples are collected.

Table 2- Overview of absolute hydrogen concentration range (minimum, maximum), measured by microcapillary cell (d_{inner}=*160 µm*), for non-deformed and plastically deformed steels (by bending and punching), after H-charging for 2 hours in 0.2 M NaOH solution containing 1 g/l thiourea

	H-charging on		
	Non-Deformed Steel	**Bended Steel**	**Punched Steel**
H (wppm)	0-0.12	0.1-0.2	0.3 – 0.9

It can be seen from table 2 that for non-deformed steel the highest calculated value (based on current measured) was 0.12 wppm of hydrogen. After the bending of the steel sheet, the average hydrogen concentration value is significantly higher, with a highest measured H-concentration of 0.2 wppm. For the punched sample, the average is even higher and the highest H-concentration measured was 0.9 wppm. These analyses suggest that bending and punching processes significantly increase the hydrogen trapping capacity of the material.

As the dimensions of the shear affected zone in the punched hole region (structure analyses details are presented in the next section) are smaller than the diameter used in the microcapillary cell measurements above (d_{inner}=160 *µm*), additional more local measurements using a micro capillary with an inner diameter of *10 µm* were performed. This very small capillary can be positioned precisely at different locations inside the shear affected zone. The corresponding positions of the capillaries (d_{inner}=160 *µm*, d_{inner}=10 *µm*) are schematically illustrated in figure 6, where the *shear affected zone* is delineated with a dashed line.

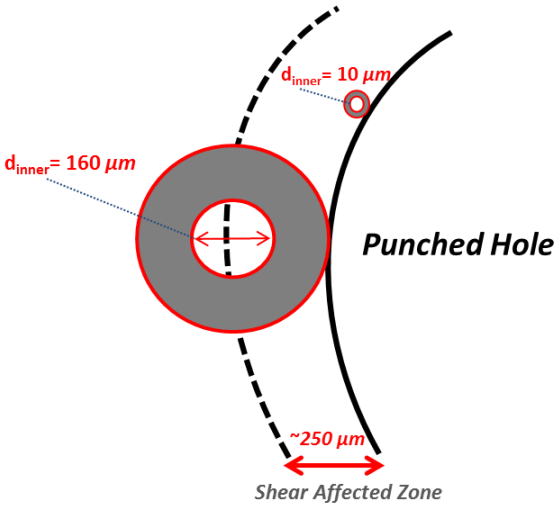

Figure 6- Schematic of the capillary cell setups with different inner diameters (160 *µm* and 10 µm) near the punched edge of the sample

Local electrochemical measurements with the 10 µm micro capillary were first done on various locations of a non H-charged punched sample, far away from the punched edge as well as inside the shear affected zone. In figure 7, the results show that the anodic current transients which define our baseline are not depending significantly on the measurement location.

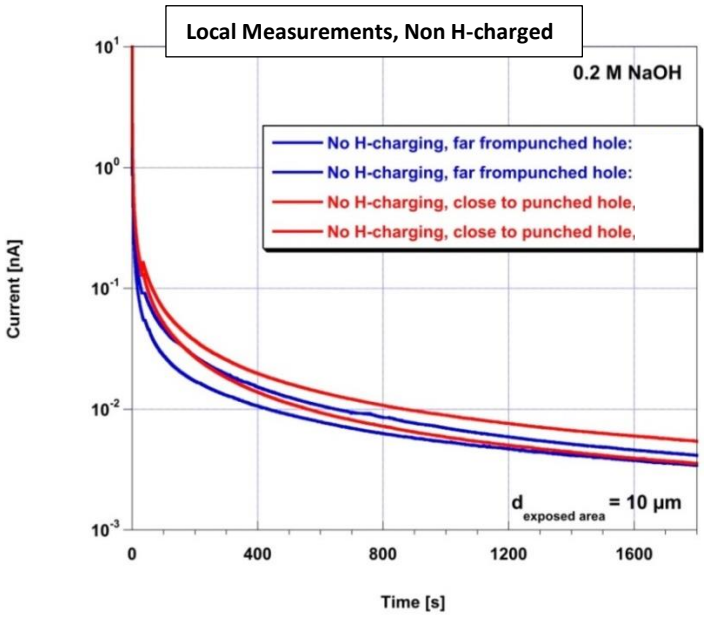

Figure 7- Overview of the anodic current transient vs. time in semi-log scale during hydrogen discharging on various locations on a non-charged sample obtained from the measurements performed by microcapillary cell (d_{inner}=*10 µm*)

The influence of H-charging is shown in figure 8 for various spots in the shear affected zone. It is clear that a much higher amount of charge is released from the H-charged sample than from the

non-charged one. This difference can be explained by the oxidation of trapped hydrogen located nearby the punched hole. Based on all the results of the local measurements shown in figure 7 and 8 and the resulting calculated hydrogen concentrations presented in figure 9, it can be stated that the obtained hydrogen concentration is distributed between the lowest H-concentration measured as 1.7 wppm, and the highest at 3.7 wppm. These local electrochemical characterizations confirm that a significantly increased amount of hydrogen can be located in the shear affected zones. One should note that for the local H-measurements, shown in Figure 9, the microcapillary cell (d_{inner}=10 μm) is positioned maximum 40 micrometer away of the punched hole.

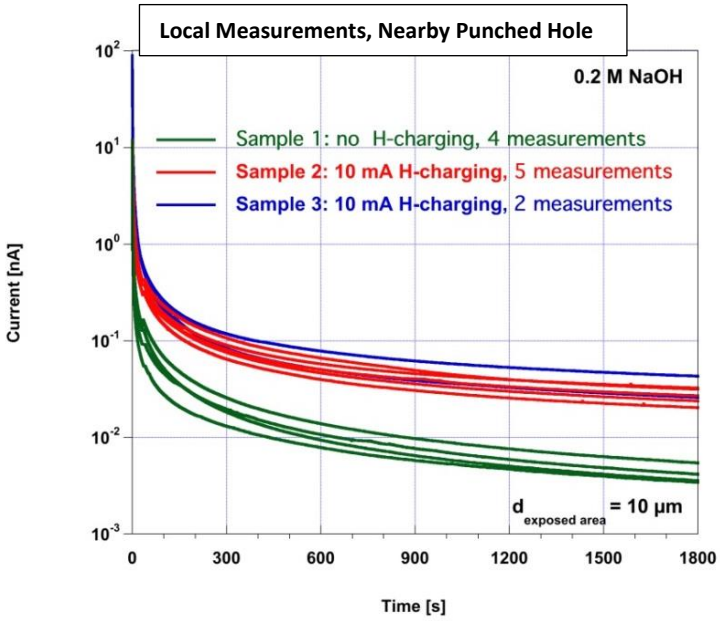

Figure 8- Overview of the anodic current transient vs. time in semi-log scale during hydrogen discharging obtained by microcapillary cell (*dinner=10 µm*) after w/o having been hydrogen charged galvanostatically at 10mA/cm^2 for 2 hours in 0.2 M NaOH solution containing 1 g/l thiourea

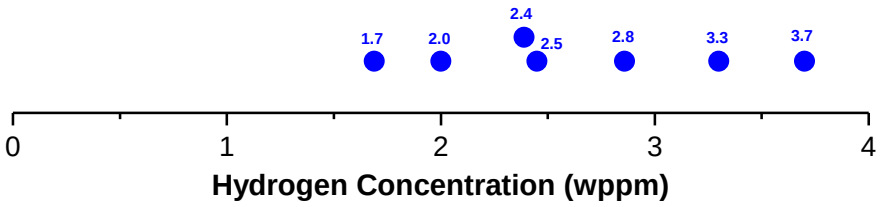

Figure 9- Estimated hydrogen concentration in the shear affected zone obtained from the measurements performed by microcapillary cell (d_{inner}=10 μm)

4.2 Microstructure and local strain analyses of a punched sample

It is known from literature that a punching process can highly deform the steel in the punched region. In figure 10.a, a punched steel sample is schematically illustrated. In figure 10.b, the near edge of the punched hole is illustrated by high magnification optical microscopy: the grains near the edge of the punched hole (up to *250 µm* away from edge) are much finer than in the bulk steel. In literature, this zone is referred to as *"shear affected zone"* where the grains are highly deformed as a result of shear stresses arising from the punching process. **[63-64]**

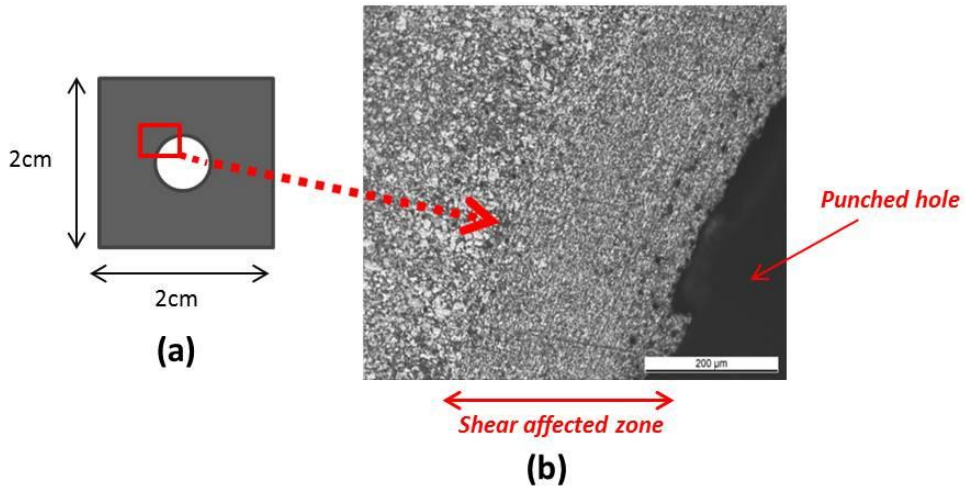

Figure 10- a) Schematic representation of a punched sample with a round hole in the middle, b) optical microscopy characterization of highly deformed region nearby the punched hole

4.2.1 SEM Analysis

The SEM images in figure 11.a, characterizing the outside of the shear affected zone, show that the ferrite grains (grey color) have a polynomial shape, and a size of about *8 µm*. Towards the punched hole, these grains become elongated and much smaller in size (*1-2 µm*), as depicted in figure 11.b and 11.c. The martensite grains (white color) are also deformed since they lost their original shape (oriented to stress direction). However, no remarkable change in their size is observed.

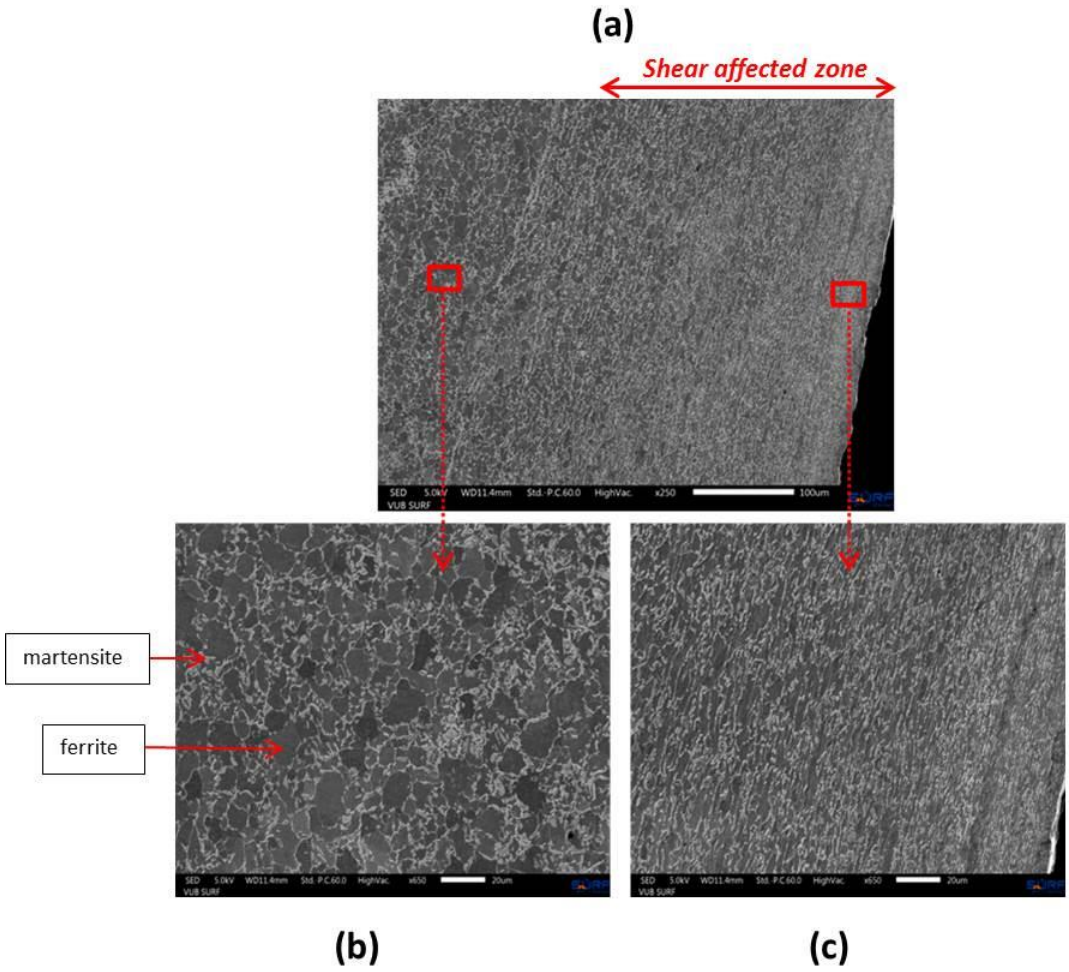

Figure 11- SEM images **a)** near the punched hole, **b)** at higher magnification outside of the shear affected region, **c)** at higher magnification within the shear affected zone

4.2.2 KAM and Strain Analysis on Punched Steel using EBSD

To quantify kernel average misorientation (KAM) and the amount of strain nearby the punched edge, EBSD analysis is carried out on four different regions (A, B, C, D), as shown in figure 12.

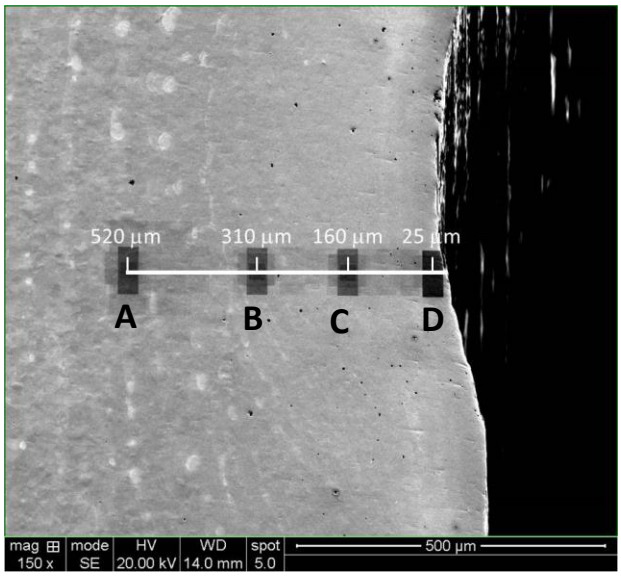

Figure 12- Illustration of the EBSD measurement regions (A, B, C and D) at distances of25µm, 160µm, 310µm and 520µm away from the punched edge

As a result of these analyses, the kernel average misorientations (KAM) with 5˚ threshold angle for each region are calculated and their corresponding maps are presented in figure 13.

For the region A, as depicted in figure 13.a, low KAM values (represented with blue color) are dominating. Going towards to the punched edge, the total fraction of low KAM values decreases in the region B as seen in figure 13.b. The decreasing trend is also continued in region C and region D, respectively. (Figure 13c-d)

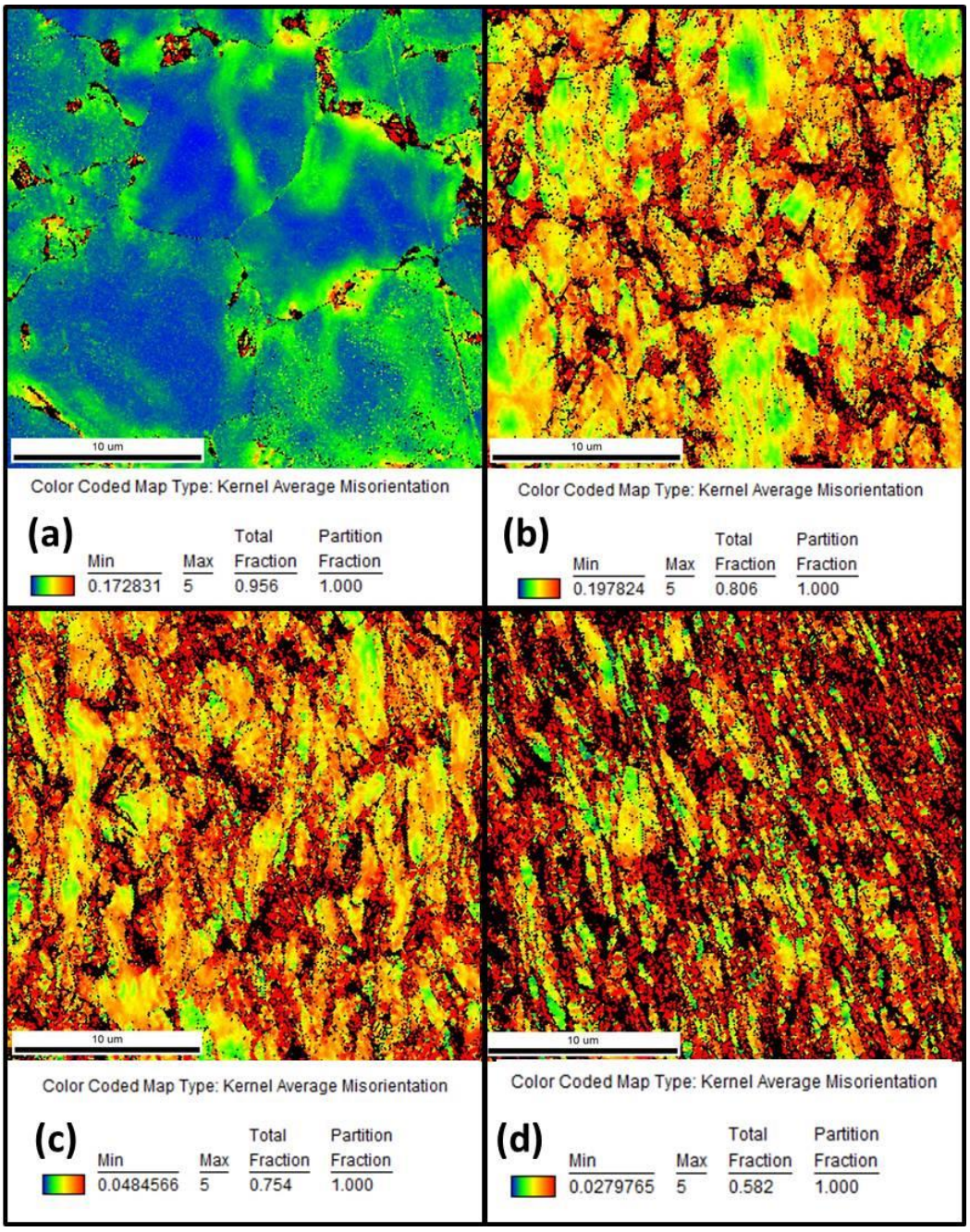

Figure 13- Kernel average misorientation maps with 5° threshold angle for a) region A, b) region B, c) region C, d) region D

The relationship between the average KAM values and equivalent strain derived based on the formula (1) is shown in figure 14.a. The main statement is that, as the average KAM values increase, the resulting equivalent strains increase. The Kernel average misorientation is considered as a measure of the dislocation density. **[53]** Consequently, together with the abovementioned increased grain boundary density, this increase in KAM implies a higher amount of potential hydrogen traps.

The corresponding equivalent strain for each region with respect to the distance from the punched edge is shown in figure 14.b.

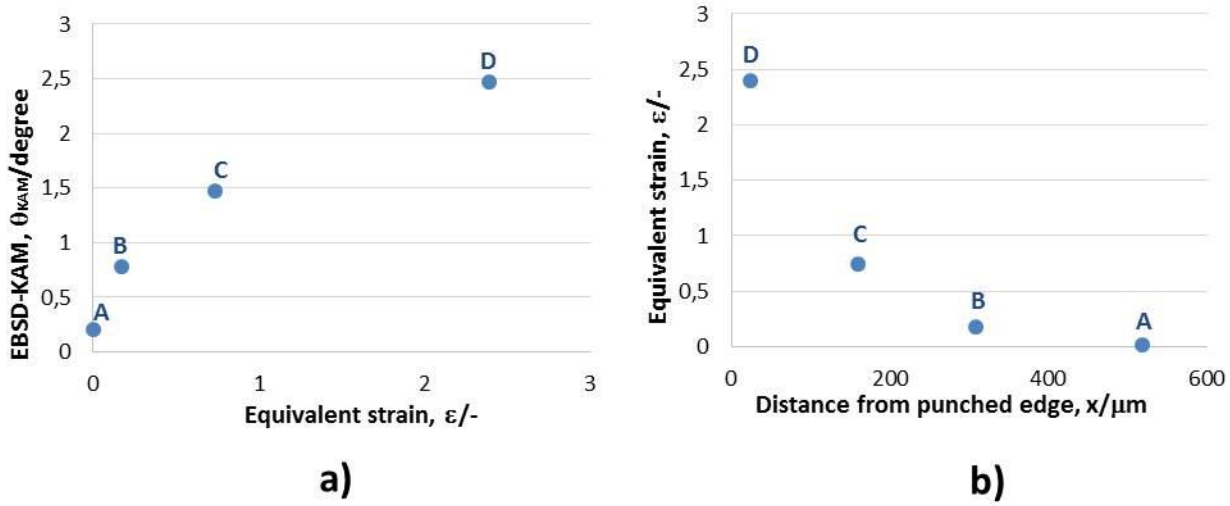

Figure 14- a) The relationship between EBSD-KAM values and the equivalent strain, b) the corresponding equivalent strain vs. the distance from the punched edge

Based on figure 14.b, the highest equivalent strain of 2.38, is localized in the region D, which is 25µm away from the punched edge. When going away from the punch border towards the interior of the steel, the equivalent strain becomes lower. Region A exhibits in fact the lowest equivalent strain of 0.01.

4.2.3 Micro-hardness Measurement

Figure 15 shows the change in hardness (measured in steps of 0.056 mm) from the edge of the punched hole to the bulk of the sample. The hardness at the punched edge is 406 HV and goes down progressively to 215 HV. At approximately a distance of 300 µm from the edge, hardness (measured up to 600 µm away from the punch border) remains at this value indicating the border of the shear affected zone.

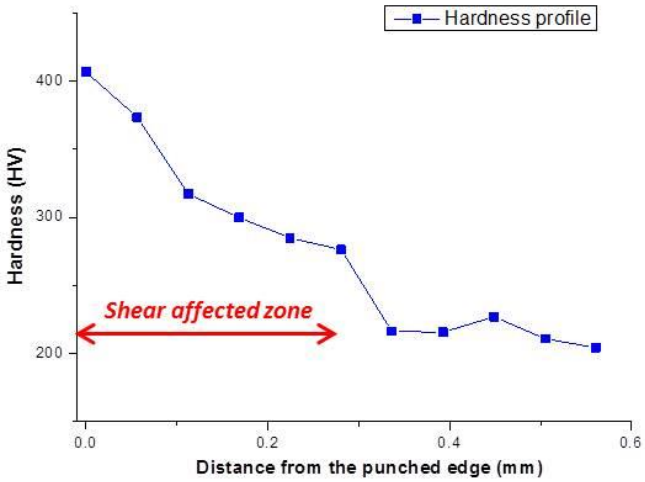

Figure 15- Vickers hardness profile of a punched steel sample as a function of distance from the edge of the punched hole

5. General Discussion

It was observed that a higher hydrogen amount can be detected in cold rolled samples or in samples strongly deformed by bending or punching compared to non-deformed steel samples. This is attributed to the higher number of traps, resulting from the applied deformation, such as a higher dislocation density and an increased amount of grain boundaries due to the grain fragmentation in the ferritic zones, where hydrogen can reside even two hours after H-charging. For instance, it was proven in our previous study on non-deformed DP600 steel that the time lag between H-charging and H-measurement can cause spontaneous H-effusion (lost for detection) of absorbed hydrogen from the steel; as such the remaining hydrogen after 100 seconds was found to be equal to 80% of its initial concentration. **[66]** Dislocations imposed by applied deformation can considerably decrease the effusion rate of hydrogen in steel **[74]** as non-deformed DP600 steel exhibit very low dislocation density. **[57] Similar effects can be assumed from the increased fraction of grain boundaries.** Considerable amount of the absorbed hydrogen in non-deformed DP600 steel is lost within the waiting period of two hours. Considering these observations and statements, it is suggested here that increasing the degree of deformation in steel can increase the amount of trapped hydrogen in the steel; **[14]** which can be measured in the regions with higher local strain, while a very low amount of hydrogen in non-deformed steel.

An increased hydrogen amount that can be trapped into a steel sample is observed as a function of the applied degree of cold deformation. This observation is in good agreement with the literature that cold-rolling can create strain zones, where hydrogen can be trapped; as such

hydrogen uptake capacity of the steel can be enhanced. **[9],[72-73], [76-77**] However, *Kapp et al.* **[59]** reported that increasing the global deformation in dual phase steel can cause a severe heterogeneity of strain distribution in its microstructure. Similarly, *Ornek et al.* **[78]** indicated that cold rolling can lead to the development of misorientation variations and gradients in the microstructure of dual phase steel, typically attributed to ''strain localization''. In general, it is accepted that strain localization is caused by the incompatible deformation between the soft ferrite matrix and the harder martensite phase showing different microstructural characteristics (shape, crystallography etc.). Considering all these statements, it can be concluded that cold-rolling can generate local strain fields of different intensity in the steel microstructure. As can be noticed from figure 5, the trapped hydrogen concentration in the 11% cold-rolled steel is distributed in the broad range from 0.1 wppm to 1.6 wppm. For 4% cold-rolled sheets, the hydrogen concentration ranges between 0.1 wppm and 0.3 wppm. This difference can be explained by the strain localization theory: local strains are more heterogeneously distributed in the microstructure of 11% cold-rolled steel, and as such there is larger heterogeneity in the local H-concentration measured by the micro-cell technique.

It is further shown that also the bending process can lead to more hydrogen trapping in the steel microstructure. This can be attributed to the increase of dislocation and grain boundary density as a result of bending. It is known from literature that shear forces are generated from bending and can highly deform the steel microstructure. Microstructural characterization of a punched sample confirms that ferrite grains become much smaller in the vicinity of the punched hole, and a shear affected zone, where excessive grain fragmentation takes place, is circumferentially located around the punched hole with a width of about *300 µm*. The micro hardness measurements also showed that the hardness of the steel becomes gradually larger when crossing the shear affected zone towards the punched edge. These observations confirm that there is severe grain fragmentation and a higher dislocation density in the shear affected zone as a result of severe work hardening, as similarly reported by *Scharf et al.* **[63-64]**.

EBSD analysis showed that EBSD-KAM values and the corresponding equivalent strain becomes higher when going towards the punched edge. This indicates that very large strain is localized there. This observation was similarly proven by *Nakada et al.* **[54]**, and in the study of *Yokoi et al.*, **[62]** it was additionally reported that local strain is heterogeneously distributed within this region due to different characteristics of ferrite and martensite phases. Considering this statement as well as our findings, it can be confirmed that very large strain and corresponding microstructural changes are heterogeneously distributed within the shear affected zone.

As mentioned earlier, the results of the measurement using the larger capillary (d_{inner}=160 µm) showed that a higher amount of hydrogen (in the range of 0.3 and 0.9 wppm) can be trapped nearby the punched hole, as compared to the non-deformed sample. However, this measurement

does not reflect the local trapped hydrogen concentration within the shear affected zone since this capillary cannot be precisely placed within this zone due to its size limits, as schematically illustrated in figure 6. As a 160 µm large capillary, in most cases, covers the outskirt of the shear affected zone, the exact hydrogen concentration within this zone cannot be determined. Conversely, using smaller capillary (d_{inner}=10 μm) dimension, the local hydrogen concentration within the shear affected zone could be determined. These results showed that much higher amounts of hydrogen (in the range of *1.7-3.7 wppm*) can be trapped in this region due to the microstructural changes that result from a high magnitude of strain. These microstructural changes, dependent on strain, are considered to be heterogeneously distributed in this region, which in turn creates a local hydrogen distribution. More importantly, our findings indicate that the shear affected zone has a higher hydrogen uptake ability, along with the presence of a large local strain in its microstructure. This can possibly make the steel very susceptible to hydrogen induced cracking since this phenomenon is believed to occur under critical hydrogen concentration in combination with a certain strain level in the literature. **[79-81]**

6. Conclusion

The microcapillary cell measurements allowed us to determine the amount of trapped hydrogen in steel with respect to the type of mechanical deformation applied. It has been demonstrated that the trapped H amount increases with the degree of cold work: a clear relationship between the deformation degree and the locally trapped hydrogen amount could be established. This indicates that mechanical deformation of steel (rolling, bending and punching) can induce more potential traps for hydrogen, compared to non-deformed steel.

Microstructural characterizations (using LOM, SEM) and micro-hardness measurements in punched steel revealed that the shear affected zone is located nearby the punched hole, where excessive grain fragmentation and higher dislocation density are observed. EBSD analysis showed that very large strain is localized in the vicinity of the punched edge. Our dedicated local measurements confirmed the presence of a locally higher amount of hydrogen within the shear affected zone, which can be considered to be critical for hydrogen embrittlement. Therefore, to assess the risk of hydrogen embrittlement with regard to local hydrogen concentration in the critical regions, local microcapillary cell measurements can be considered as a promising technique.

Acknowledgements

The authors gratefully acknowledge AVN (Association Vinçotte Nuclear) for the financial support of this PhD project as well as the esteemed European Federation of Corrosion (EFC) for the Young Scientist grant that supported this collaboration between VUB and EMPA. The authors further wish to thank the Special Research Fund (BOF), UGent (BOF15/BAS/06) and the UGent postdoctoral fellowship via grant nr BOF01P03516. We would also like to thank postdoctoral researcher Ege Dundar at Vrije Universiteit Brussel (VUB) as well as several postdoctoral researchers of EMPA, Sebastian Siol, Noemie Ott, Yeliz Unutulmazsoy and PhD student Emilija Ilic for the valuable discussions. Lastly, thanks go to Bart Lippens and Oscar Steenhaut for the many steel sample preparations for the electrochemical experiments as well as for the assistance with the scanning electron microscopy (SEM).

References:

[1]: G. Lovicu, M. Bottazzi, F. D'Aiuto, M. De Sactis, A. Dimatteo, C. Santus and R. Valentini, *"Hydrogen embrittlement of automotive advanced high-strength steels"*, Metallurgical and Materials Transaction A, Vol. 43A, pp. 4075-4087 , (2012)

[2]: Q. Liu, E. Gray, J. Venezuela, Q. Zhou, C. Tapia-Bastidas, M. Zhang, and A. Atrens, *"Equivalent hydrogen fugacity during electrochemical charging of 980DP steel determined by thermal desorption spectroscopy"*, Advanced Engineering Materials, Vol. 1700469, pp. 1-13, (2017)

[3]: T. Depover, E. Wallaert and K. Verbeken, *"Fractographic analysis of the role of hydrogen diffusion on the hydrogen embrittlement susceptibility of DP steel"*, Materials Science&Engineering A, Vol. 649, pp. 201-208, (2016)

[4]: G. Katano, K. Ueyema, and M. Mori, *"Observation of hydrogen distribution in high-strength steel"*, Journal of Materials Science, Vol. 36, pp. 2277-2286, (2001)

[5]: Turnbull, A., *"Perspectives on hydrogen uptake, diffusion and trapping"*, International Journal of Hydrogen Energy, 40(47), pp. 16961–16970, (2015)

[6]: M. Dadfarnia, P. Sofronis, and T. Neeraj, *"Hydrogen interaction with multiple traps: Can it be used to* mitigate *embrittlement?"*, International Journal of Hydrogen Energy, Vol. 36, pp. 10141-10148, (2011)

[7]: M. Wang, E. Akiyama, and K. Tsuzaki, *"Effect of hydrogen on the fracture behaviour of high strength 372 steel during slow strain rate test"*, Corrosion Science, Vol. 49, pp. 4081-4097, (2007)

[8]: M. Koyama, E. Akiyama, and K. Tsuzaki, *"Effect of hydrogen content on the embrittlement in a Fe-Mn-374 C twinning-induced plasticity steel"*, Corrosion Science, Vol. 59, pp. 277-281, (2012)

[9]: R. A. Oriani, *"The diffusion and trapping of hydrogen in steel"*, Acta Metall, Vol. 18, pp. 147, (1970)

[10]: R.L.S. Thomas, D. Li, R.P. Gangloff, and J.R. Scully, *"Trap-governed hydrogen diffusivity and uptake capacity in ultrahigh-strength AERMET 100 steel"*, Metallurgical and Materials Transaction A, Vol. 33A, pp. 1991-2002, (2002)

[11]: T. Zakroczymski, *"The Effect of Straining on the Transport of Hydrogen in Iron, Nickel, and Stainless Steel"*, Corrosion, Vol. 41, pp. 485-489, (1985)

[12]: J.P. Hirth, *"Effects of hydrogen on the properties of iron and steel"*, Metallurgical Transactions A, Vol. 11, pp. 861-890, (1980)

[13]: J. Petit J, P. Scott, "*Comprehensive structural integrity – fracture of materials from nano to macro"*, Elsevier, Vol. 6, pp. 65–101, (2003)

[14]: A.J. Kumnick, and H.H. Johnson, *"Deep trapping states for hydrogen in deformed iron"*, Acta Metallurgica, Vol. 28, pp. 33-39, (1979)

[15]: T. Depover T, K. Verbeken, *"The detrimental effect of hydrogen at dislocations on the hydrogen embrittlement susceptibility of Fe-C-X alloys: An experimental proof of the HELP mechanism"*, International Journal of Hydrogen Energy, Vol. 43, pp. 3050-3061, (2018)

[16]: W. Krieger, S. V. Merzlikin, A. Bashir, A. Szczepaniak, H. Springer, and M. Rohwerder, *"Spatially resolved localization of trapped hydrogen in zero to three dimensional defects inside ferritic steel"*, Acta Materialia, Vol. 144, pp. 235-244, (2018)

[17]: M. Merklein, J.M. Allwood, B.A. Behrens, A. Brosius, H. Hagenah, K. Kuzman, K. Mori, A. E. Tekkaya, A. Weckenmann, *"Bulk forming of sheet metal",* CIRP Annals-Manufacturing Technology, Vol. 61, pp. 725-745, (2012)

[18]: S. Takagi, Y. Toji, M. Yoshino and K. Hasegawa, "Hydrogen embrittlement resistance evaluation of ultra-high strength steel sheets for automobiles", ISIJ International, Vol. 52, No. 2, pp. 316-322, (2012)

[19]: T. Depover and K. Verbeken, *"The effect of TiC on the hydrogen induced ductility loss and trapping behavior of Fe-C-Ti alloys "*, Corrosion Science, Vol. 112, pp. 308 (2016).

[20]: T. Depover and K. Verbeken, *"Evaluation of the effect of V4C3 precipitates on the hydrogen induced mechanical degradation in Fe-C-V alloys"*, Materials Science and Engineering A, Vol. 675, pp. 299 (2016).

[21]: T. Depover, E. Wallaert, and K. Verbeken, *"Hydrogen trapping and hydrogen induced mechanical degradation in lab cast Fe-C-Cr alloys"*, Materials Science and Engineering A, Vol. 669, pp. 134 (2016).

[22]: T. Depover and K. Verbeken, *"Evaluation of the role of Mo2C in hydrogen induced ductility loss in Q&T Fe-C-Mo alloys"*, International Journal for Hydrogen Energy, Vol. 41, pp. 14310 (2016).

[23]: T. Depover, O. Monbaliu, E. Wallaert, and K. Verbeken, *"Effect of Ti, Mo and Cr Based Precipitates on the Hydrogen Trapping and Embrittlement of Fe-C-X Q&T Alloys"*, International Journal of Hydrogen Energy, Vol. 40, pp. 16977 (2015)

[24]: D. Perez Escobar, L. Duprez, A. Atrens and K. Verbeken, *"Influence of experimental parameters on thermal desorption spectroscopy measurements during evaluation of hydrogen trapping"*, Journal of Nuclear Materials, Vol. 450, pp. 32-41, (2014)

[25]: M. Koyama, A. Bashir,M. Rohwerder, S. V.Merzlikin, E. Akiyoma, K. Tsuzaki, and D. Raabe, *"Spatially and kinetically resolved mapping of hydrogen in a twinning induced plasticity steel by use of scanning kelvin probe force microscopy"*, Journal of the Electrochemical Society, Vol. 12, pp. 638 (2015)

[26]: E. Akiyama, K.Matsukado, M.Wang, and K. Tsuzaki, *"Evaluation of hydrogen entry into high strength steel under atmospheric corrosion"*, Corrosion Science, Vol. 52, pp. 2758 (2010)

[27]: T. Depover, E. Wallaert and K. Verbeken, *"On the synergy of diffusible hydrogen content and hydrogen diffusivity in the mechanical degradation of laboratory cast Fe-C alloys"*, Materials Science and Technology A, Vol. 664, pp. 195-205, (2016)

[28]: D. Perez Escobar, L. Duprez, A. Atrens and K. Verbeken, *"Influence of experimental parameters on thermal desorption spectroscopy measurements during evaluation of hydrogen trapping"*, Journal of Nuclear Materials, Vol. 450, pp. 32-41, (2014)

[29]: M. A. V. Devanathan, *"The Adsorption and Diffusion of Electrolytic Hydrogen in Palladium"*, Proc. Royal Soc. London Ser. A – Math. Phys. Sci., Vol. 270, pp. 90 (1962).

[30]: B. G. Pound, "Hydrogen trapping in high-strength steels", Acta Metal, Vol. 46, pp.5733, (1998)

[31]: M. Y. Chi, Y. F.Wu, J. K.Wu, and D.-Y. Lin, *"Hydrogen embrittlement susceptibility and permeability of two high strength steels"*, Corrosion Science, Vol. 48, pp. 1926 (2006)

[32]: E. Fallahmohammadi, F.Bolzoni, and L. Lazari, *"Measurement of lattice and apparent diffusion coefficient of hydrogen in X65 and F22 pipeline steels"*, International Journal of Hydrogen Energy, Vol. 38, pp. 2531 (2013)

[33]: E. Van den Eeckhout, A. Laureys, Y. Van Ingelgem and K. Verbeken, *"Hydrogen permeation through deformed and heat-treated Armco pure iron"*, Materials Science and Technology, Vol. 33, pp. 1515-1523, (2017)

[34]: M. Yan and Y.Weng, *"Study on hydrogen absorption of pipeline steel under cathodic charging"*, Corrosion Science, Vol. 48, pp. 432 (2006)

[35]: J. Capelle, I. Dmytrakh, and G. Pluvinage, *"Comparative assessment of electrochemical hydrogen absorption by pipeline steels with different strength"*, Corrosion Science,Vol. 52, pp. 1554 (2010)

[36]: F. Mansfeld, "*Electrochemical determination of hydrogen in steel*", Proceedings of the ARPA/AFML Review of Progress in Quantitative NDE, Vol. 16, (1978)

[37]: B. Ozdirik, K. Baert, T. Depover, J. Vereecken, K. Verbeken, H. Terryn, and I. De Graeve, "*Development of an electrochemical procedure for monitoring hydrogen sorption/desorption in steel*", Journal of Electrochemical Society, Vol.164, pp. 747-757, (2017)

[38]: N. Saintier, T. Awane, J.M. Olive, S. Matsuoka, Y. Murakami, *"Analyses of hydrogen distribution around fatigue crack on type 304 stainless steel using secondary ion mass spectrometry"*, Int. Hydrogen Energy, Vol. 36, pp. 8630-8640, (2011)

[39]: M. Koyama, M. Rohwerder, C. C. Tasan, A. Bashir, A. Akiyama, K. Takaif, D. Raabe, and K. Tsuzaki, *''Recent progress in microstructural hydrogen mapping in steels: quantification, kinetic analysis, and multi-scale characterization''*, Materials Science and Technology, Vol.33, No. 13, pp. 1481-1496, (2017)

[40]: T. Suter, H. Böhni, Proceedings of the 12th International Corrosion Congress, Vol. 3A, Houston TX, pp. 1367, (1993)

[41]: T. Suter, T. Peter, H. Böhni, *"Electrochemical methods in corrosion research V"*, in: M.G.S. Ferreira, A.M.P. Simoes (Eds.), Materials Science Forum Proceedings, vols. 192–194, pp. 25,Trans. Tech Publications, Uetikon, Switzerland, **(**1994)

[42]: H. Böhni, T. Suter, A. Schreyer, *"Microtechniques and nanotechniques to study localized corrosion"*, Electrochimica Acta, Vol.40, pp. 1361-1368, (1995)

[43]: T. Suter, H. Böhni, *"Microelectrodes for corrosion studies in microsystems"*, Electrochimica Acta, Vol. 47, pp. 191-199, (2001)

[44]: F. Andreatta, L. Fedrizzi, *''The use of the electrochemical micro-cell for the investigation of corrosion phenomena"*, Electrochimica Acta, Vol. 203, pp. 337-349, (2016)

[45]: S. Kühn, F. Unterumsberger, T. Suter, and M. Pohl, *"Neue Methoden zur Analyse von diffusiblem Wasserstoff in hochfesten Stählen"*, Journal of Materials Testing, Vol. 55, No. 9, pp. 648-652, (2013)

[46]: G. Manke, J. Jurgensen, M. Pohl, *"Development of an in-situ Measuring Cell to non-destructive, local measurement of diffusible hydrogen content in steels"*, International Hydrogen Conference 2016, pp. 440-445

[47]: J. Shinozaki, I. Muto, T. Omura, M. Numata, and N. Hara, *"Local dissolution of MnS inclusion and microstructural distribution of absorbed hydrogen in carbon steel"*, Journal of Electrochemical Society, Vol. 158, pp. 302-309, (2011)

[48]: K. Fushimi, M. Jin, Y. Kitagawa, T. Nakanishi, and Y. Hasegawa, *"Hydrogen permeation into a carbon steel sheet observed by a micro-capillary combined with a devanathan-stachurski cell"*, ISIJ International, Vol. 56, No. 3, pp. 431-435, (2016)

[49]: M. Koyama, H. Springer, S.V. Merzlikin, K. Tsuzaki, E. Akiyama, and D. Raabe, *"Hydrogen embrittlement associated with strain localization in a precipitation-hardened FeMnAlC light weight austenitic steel"*, International Journal of Hydrogen Energy, Vol. 39, pp. 4634-4646, (2014)

[50]: T. Michler, C. San Marchi, J. Naumann, S. Weber, M. Martin, *"Hydrogen environment embrittlement of stable austenitic steels"*, International Journal of Energy, Vol. 37, pp. 16231-16246, (2012)

[51]: S.I. Wright, M.M. Nowell, and D.P. Field, *"A review of strain analysis using electron backscatter diffraction"*, Microsc. Microanal., Vol. 17, pp. 316-329, (2011)

[52]: A.J. Wilkinson, T.B. Britton, J. Jiang, and P.S. Karamched, *"A review of advances and challenges in EBSD strain mapping"*, IOP Conf. Series: Materials Science and Engineering, Vol. 55, pp. 1-9, (2014)

[53]: L.N. Brewer, D.P. Field, C.C. Merriman, *"Mapping and assessing plastic deformation using EBSD"*, Ed: A.J. Schwartz, M. Kumar, B.L. Adams, D.P. Field, Electron backscatter diffraction in material science, Springer Science & Business Media, (2000)

[54]: N. Nakada, K. Ikeda, H. Shuto, T. Yokoi, T. Tsuchiyama, S. Hata, H. Nakashima and S. Takaki, *"Quantification of large deformation with punching in dual phase steel and change of its microstructure – part 2: Local strain mapping of dual phase steel by a combination technique of electron backscatter diffraction and digital image correlation methods"*, ISIJ International, Vol. 56, No. 11, pp. 2077-2083, (2016)

[55]: J. Malina, A. B. Hadzipasic and S. Niznik, *"Electrochemical corrosion and hydrogen diffusivity in dual phase steel"*, Zastita Materija, Vol. 54, pp. 130-134, (2013)

[56]: G. Avramovic-Cingara, Y. Ososkov, M. K. Jain and D. S. Wilkinson, *"Effect of martensite distribution on damage behaviour in DP600 dual phase steels"*, Materials Science and Engineering A, Vol. 516, pp. 7-409 16, (2009)

[57]: Korzekwa, D.A., D.K. Matlock, and G. Krauss, *"Dislocation substructure as a function of strain in a dual-phase steel"*, Metallurgical Transactions A, Vol. 15A, p. 1221- 1228, (1984)

[58]: M. Ruiz-Andres, A. Conde, J. de Damborenea, I. Garcia, *"Microstructural and Micromechanical Effects of Cold Roll-forming on High Strength Dual Phase Steels"*, Materials Research, Vol. 18, pp. 843-852, (2015)

[59]: M. Kapp, T. Hebesberger, O. Kolednik, *''A micro-level strain analysis of a high-strength dual-phase steel''*. Int. J. Mater. Res. Vol.102, pp. 687–691, (2011)

[60]: M. Yoshino, Y. Toji, S. Takagi, and K. Hasegawa, *"Influence of sheared edge on hydrogen embrittlement resistance in an ultra-high strength steel sheet"*, ISIJ International, Vol. 54, No. 6, pp. 1416-1425, (2014)

[61]: X. Wu, H. Bahmanpour, K. Schmid, *"Characterization of mechanically sheared edges of dual phase steels"*, Journal of Materials Processing Technology, Vol. 212, pp. 1209-1224, (2012)

[62]: T. Yokoi, H. Shuto, K. Ikeda, , T. Tsuchiyama, T. Ohmura, Y. Mine and K. Takashima, *"Quantification of large deformation with punching in dual phase steel and change of its microstructure –part 1: Proposal of quantification technique of the punching damage of the dual phase steel"*, ISIJ International, Vol. 56, No. 11, pp. 2068-2076, (2016)

[63]: R. Scharf, A. Muhr, G. Luckeneder, P. Larour, M. Mraczek, J. Rehrl, F. Leomann, K.-H. Stellnberger, J. Faderl and G. Mori, *"Hydrogen embrittlement of DP-1000 flat steel sheet: Influence of mechanical properties, specimen geometry, pre-damaging and electrolytically zinc galvanizing"*, Materials and Corrosion, Vol. 67, No. 3, (2016)

[64]: R. Scharf, A. Muhr, K.-H. Stellnberger, J. Faderl, C. Holzer and G. Mori, *"Hydrogen embrittlement of high strength steel under in situ corrosive charging conditions and tensile load"*, Materials and Corrosion, Vol. 68, No. 1, (2017)

[65]: T. Depover, E. Wallaert and K. Verbeken, *"Fractographic analysis of the role of hydrogen diffusion on the hydrogen embrittlement susceptibility of DP steel"*, Materials Science&Engineering A, Vol. 649, pp. 201-208, (2016)

[66]: B. Ozdirik, T. Depover, L. Vecchi, K. Verbeken, I. De Graeve, *"Comparison of electrochemical and thermal evaluation of hydrogen uptake in steel alloys having different microstructures"*, Journal of Electrochemical Society, Vol. ??, pp. ??, (2018)

[67]: M. Breimesser, S. Ritter, H.P. Seifert, S. Virtanen and T. Suter, *"Application of the electrochemical microcapillary technique to study intergranular stress corrosion cracking of austenitic stainless steel on the micrometer scale"*, Corrosion Science, Vol. 55, pp. 126-132, (2012)

[68]: G. Avramovic-Cingara, Y. Ososkov, M. K. Jain and D. S. Wilkinson, *"Effect of martensite distribution on damage behaviour in DP600 dual phase steels"*, Materials Science and Engineering A, Vol. 516, pp. 7-16, (2009)

[69]: Z. Szklarska-Smialowska and Z. Xia, *"Hydrogen trapping by cold-worked X-52 steel"*, Corrosion Science, Vol. 39, No. 12, pp. 2171-2180, (1997)

[70]: W. Dietzel, M. Pfuff, and G.G. Juilfs, *"Hydrogen permeation in plastically deformed steel membranes"*, Materials Science, Vol. 42, pp. 78-84, (2006)

[71]: A.-M. Brass, F. Guillon, and S. Vivet, *"Quantification of hydrogen diffusion and trapping in 2.25Cr-1Mo and 3Cr-1Mo-V Steels with the electrochemical permeation technique and melt extractions"*, Metallurgical and Materials Transactions A, Volume 35A, pp. 1449-1464, (2004)

[72]: Y. Huang, A. Nakajima, A. Nishikata, and T. Tsuru, *"Effect of mechanical deformation on permeation of hydrogen in iron"*, ISIJ International, Vol. 43, pp. 548-554, (2003)

[73]: H. Huang and W.J.D. Shaw, *"Hydrogen embrittlement interactions in cold-worked steel"*, Corrosion Science, Vol. 51, pp. 30-36, (1995)

[74]: A.M. Brass, M. Garet, A.L. Etter, "Hydrogen absorption and diffusion in Cr-Mo low alloy steels undergoing tensile straining", Hydrogen at Surface and Interfaces: Proceedings of the International Symposium, Electrochemical Society Proceedings, Vol. 16, (2000)

[75]: L.J. Qiao, J.L. Luo, and X. Mao, *"Hydrogen evolution and enrichment around stress corrosion crack tips of pipeline steels in dilute bicarbonate solutions"*, Corrosion, Vol. 54, pp. 115-120, (1998)

[76]: G. M. Pressouyre and I. M. Bernstein, *"An example of the effect of hydrogen trapping on hydrogen embrittlement''*, Metallurgical Transactions A, Vol. 12A, pp. 835-844, (1981)

[77]: G. W. Hong and J. Y. Lee, *"The interaction of hydrogen with dislocation in iron"*, ACTA Metallurgica, Vol. 32, pp. 1581-1589, (1984)

[78]: C. Ornek, D.L. Engelberg, *"SKPFM measured Volta potential correlated with strain localization in microstructure to understand corrosion susceptibility of cold-rolled grade 2205 duplex stainless steel"*, Corrosion Science, Vol. 99, pp. 164-171, (2015)

[79]: A. E. Schuetz and W.D Robertson, *"Hydrogen Absorption, Embrittlement And Fracture of Steel"*, CORROSION, Vol. 13, pp. 33-54, (1957)

[80]: J. Venezuela, Q. Liu, M. Zhang, Q. Zhou and A. Atrens, *"The influence of hydrogen on the mechanical and fracture properties of some martensitic advanced high strength steels studied using the linearly increasing stress test"*, Corrosion Science, Vol. 99, pp. 98-117, (2015)

[81]: M. Koyama, E. Akiyama, K. Tsuzaki, *"Effect of hydrogen content on the embrittlement in a Fe-Mn-C twinning-induced plasticity steel"*, Corrosion Science, Vol. 59, pp. 277-281, (2012)